

Noble Gas Planetology and the Xenon Clouds of Uranus

KEVIN ZAHNLE¹

¹*NASA Ames Research Center
Mail Stop 245-3
Moffett Field, CA 94043, USA*

(Received October 31, 2023; Revised January 22, 2024; Accepted February 6, 2024)

Submitted to *Planetary Science Journal*

ABSTRACT

Noble gases provide tracers of cosmic provenance that are accessible to a future Uranus Atmospheric Probe. Argon and krypton are expected to be well-mixed on Uranus with respect to H₂ and He, although condensation at the winter pole may be possible. The Ar/H₂ and Ar/Kr ratios address whether the materials accreted by Uranus resembled the extremely cold materials accreted by Jupiter's atmosphere, or whether they were warmer like comet 67P/Churyumov-Gerasimenko, or whether Uranus is like neither. Xenon condenses as an ice, probably on methane ice, in Uranus's upper troposphere. Condensation may complicate interpretation of Xe/H₂, but it also presents an opportunity to collect concentrated xenon samples suitable for measuring isotopes. Solar System Xe tracks three distinct nucleosynthetic xenon reservoirs, one evident in the Sun and in chondritic meteorites, a second in refractory presolar grains, and a third evident in comet 67P/C-G and in Earth's air. The first and third reservoirs appear to have been captured from different clouds of gas. The two gases do not appear to have been well-mixed; moreover, the high ¹²⁹Xe/¹³²Xe ratio in 67P/C-G implies that the gas was captured before the initial nucleosynthetic complement of ¹²⁹I (15.7 Myr half-life) had decayed. Xenon's isotopic peculiarities, if seen in Uranus, could usefully upset our understanding of planetary origins. Krypton's isotopic anomalies are more subtle and may prove hard to measure. There is a slight chance that neon and helium fractionations can be used to constrain how Uranus acquired its nebular envelope.

Keywords: Uranus(1751) — Solar System (1528) — Chemical abundances(224) — Isotopic abundances(867) — Atmospheric clouds(2180)

1. INTRODUCTION

Noble gases play an outsized role in comparative planetology. Their value stems from their volatility and chemical inertness: the vast majority of a planet’s noble gases are likely to be found in its atmosphere, and hence are relatively accessible to spacecraft measurements, while their simple geochemistry gives hope that we can understand what they are doing. Moreover, noble gases often display big signals, both in relative elemental abundances and in isotopic structures within an element.

Any Uranus Atmospheric Probe worth flying will attempt to obtain elemental and isotopic abundances of the noble gases. Noble gases provide most of the spacecraft-accessible tracers of the materials Uranus was made from. In particular, noble gas elemental abundances can tell us if Uranus’s atmosphere accreted from extremely cold ices similar to what we see as vapor in Jupiter’s atmosphere, or whether it accreted from warmer materials akin to the comet 67P/Churyumov-Gerasimenko, or whether it accreted from something else again (Mandt et al. 2020). Noble gases can also tell us about the history, composition, and evolution of the solar nebula (Mandt et al. 2020). Xenon’s isotopes in particular can tell us if Uranus accreted from the same mix of interstellar gases as the Sun or if, like Earth’s air or 67P/C-G, it records a different provenance. On a bigger scale, noble gases provide a test of the convenient metallicity hypothesis—the hypothesis that all elements heavier than helium are equally enriched in gas giants—by assessing the “metals” in the cold gas giants of our own Solar System. Is uniform metallicity a general property of gas giants, including exoplanets, or do we extrapolate too much from Jupiter?

This essay opens with a discussion of how Jupiter’s atmophiles and the composition of 67P/C-G can be used to predict the noble gases of Uranus. We next address the heretofore overlooked likelihood that xenon condenses on Uranus. Third, we review the strangely huge isotopic anomalies seen in solar system xenon and how the different kinds of Xe are traced back to genetically distinct pools of cosmic gas. In two brief appendices, we ask if neon could be fractionated by nebular escape, and we provide a heuristic derivation of U-Xe, the original base composition of the Xe in Earth’s atmosphere. U-Xe provides a link between Earth’s air and the outer solar system.

2. URANIAN NOBLE GASES: TWO EXEMPLARY CASES

2.1. *Uranus inspired by Jupiter*

NASA’s Galileo Probe found that Jupiter’s atmosphere contains six of the most volatile elements—C, N, S, Ar, Kr, and Xe—at abundances that are roughly $2.5\times$ what they are in a solar composition gas (Owen et al. 1999; Mahaffy et al. 2000; Atreya et al. 2003; Wong et al. 2004; Mandt et al. 2020). The Jovian data normalized to solar composition are shown in Figure 1. Carbon, nitrogen, and sulfur are chemically active and form a great variety of compounds that can be rather abundant in volatile-rich meteorites. Argon, krypton, and xenon are noble gases that do no such thing. The plausible way to get a nearly uniform enhancement of three chemically active volatile elements and three chemically inactive volatile elements is to quantitatively freeze out all six as ices (Owen et al. 1999). Owen et al. (1999) therefore proposed that there must have existed, and may still exist, a significant population of bodies in the solar system that condensed at temperatures cold enough to freeze out all the elements other than H, He, and Ne. The cold bodies need not have been large. Snowballs or pebbles could suffice, provided only that the solids were big enough to separate aerodynamically from the gas (Cuzzi and Zahnle 2004; Guillot and Hueso 2006). Whatever form the cold matter took, the mass involved must have been enormous to make a major contribution to a planet as big as Jupiter. Hence a reasonable null hypothesis is to expect a similar noble gas pattern on Uranus, scaled up from Jupiter in proportion to the observed abundance of methane.

With these considerations in mind, we have updated Owen et al. (1999)’s plot of Jovian C, N, S, Ar, Kr, and Xe abundances and extended it to encompass Uranus. These are the subjects of Figure 1. The best available data for Uranus are for He and CH_4 , as both are abundant enough to strongly affect the atmospheric scale height, which is the quantity that was measured (Lindal et al. 1987; Sromovsky et al. 2011). Because the scale height depends on the ratio of temperature to mean molecular weight, the retrieved He and CH_4 abundances are degenerate with temperature. Retrieval therefore exploits methane condensation as a temperature constraint. Sromovsky et al. (2011)’s preferred deep methane abundance of 2.3-4% is consistent with highly variable (because methane condenses) telescopic measurements of mixing ratios of 1-5% (Moses et al. 2020). Assuming a solar He/H ratio, methane concentrations of 2-5% correspond to C/ H_2 enhancements of 60 ± 25 . The corresponding He/ H_2 volume mixing ratio is $15 \pm 1\%$.

Possible Uranian Ar, Kr, and Xe abundances are scaled from Jupiter at a nominal enhancement of $50\times$, but over a very wide range extending from the small $2.5\times$

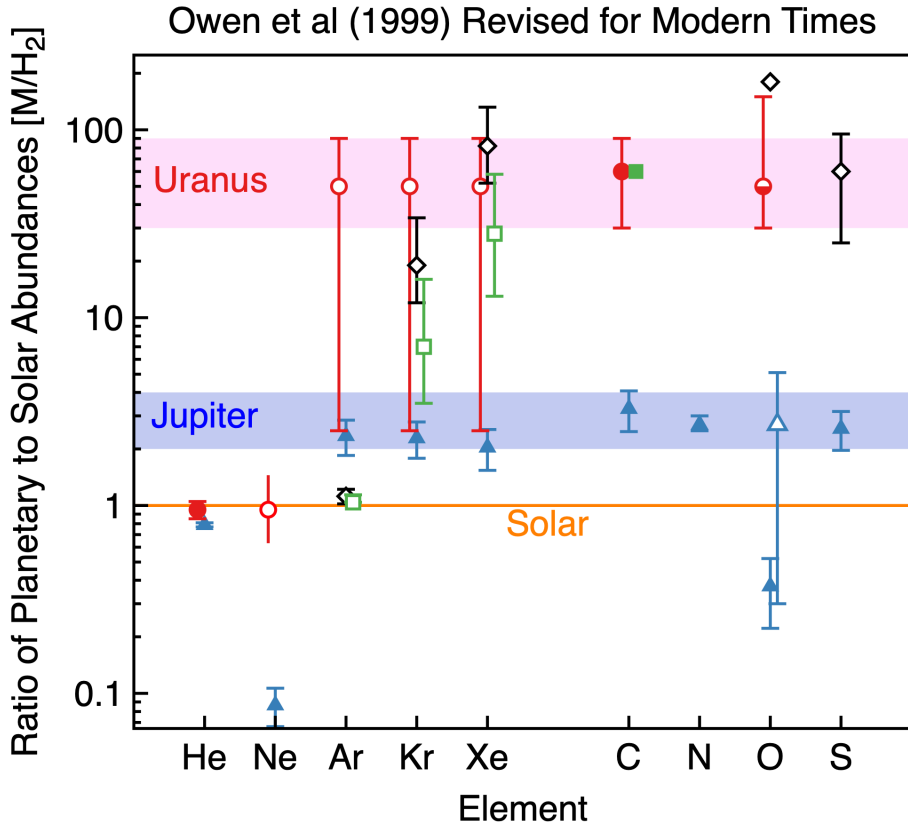


Figure 1. Imagining noble gas abundances of Uranus. Jovian data (filled blue triangles) have been updated from von Zahn and Hunten (1996), Mahaffy et al. (2000), and Wong et al. (2004). The data are plotted as ratios to solar abundances (Lodders 2020). For the jovian N/H₂ ratio, we use an NH₃ abundance of 340^{+27}_{-17} ppmv (Moeckel et al. 2023), to which we add the putative NH₄SH cloud using H₂S as reported by the Galileo Probe (Wong et al. 2004). The open blue triangle is a Juno inference of equatorial H₂O (Li et al. 2020). The Uranian C/H₂ ratio is from CH₄ (red filled disk), which presents variable deep atmospheric volume mixing ratios of order 2-5% (Sromovsky et al. 2011), corresponding to a metallicity enhancement of 60 ± 25 . An O/H₂ ratio (red half-filled disk) is inferred from thermochemical quenching theory (Venot et al. 2020). One set of hypothetical Uranian abundances of Ar, Kr, and Xe is scaled with C from Jupiter (open red circles). Another set is scaled from abundances in comet 67P/Churyumov-Gerasimenko assuming a solar C/O ratio (open green squares). A third set is scaled from volatile C abundances in 67P/C-G (open black diamonds, using data tabulated by Mandt et al. (2020)). In this case we have arbitrarily plotted S but not N. For clarity, points are plotted with small artificial shifts along the x-axis.

jovian amplification to an upper bound of $100\times$. We have not scaled NH_3 or H_2S from Jupiter, as neither behave simply enough at Uranian temperatures to yield trustworthy bulk abundances from remote observations (Guillot 2019). Nitrogen and sulfur will be targets for *in situ* measurements with the Uranus Probe.

Oxygen is not among the six super-volatile elements— H_2O is much too refractory. The Galileo Probe saw relatively little water (Wong et al. 2004). Juno microwave retrievals of H_2O at Jupiter’s equator, where the NH_3 abundance is high and relatively uniform, suggest that H_2O may be amplified above solar by a factor $2.7^{+2.4}_{-1.7}$ (Li et al. 2020). This new datum is plotted as an open triangle on Figure 1. Recent theoretical thermochemistry quenching calculations suggest that Uranian O/H is enhanced some $45\times$ above the solar ratio (Venot et al. 2020), which revises a previous estimate of $150\times$ obtained by the same group (Cavalié et al. 2017). We have plotted Uranian O/ H_2 on Figure 1 at $50\times$ solar with generous uncertainties.

As stressed above, the simplest way to separate C, N, S, Ar, Kr, and Xe from H_2 and He is to invoke temperatures cold enough that all the elements other than H_2 , He, and Ne freeze out quantitatively. Once this is done, there are several plausible ways to separate the cold solids from the nebular gas. Figure 2 illustrates some of these.

1. H, He, and Ne can be photo-evaporated by EUV irradiation of the nebula (Hollenbach et al. 2000; Guillot and Hueso 2006). This increases the solid/gas ratio of the matter left behind. A high solid/gas ratio promotes the aggregation of planetesimals by gravito-aerodynamic processes, such as the streaming instability (Youdin and Goodman 2005) or turbulent concentration (Estrada et al. 2016). The distant planetesimals could later be scattered and caught by the expansive envelopes of growing giant planets (Pollack et al. 1996), enriching their atmospheres.
2. The icy pebbles or snowballs can spiral inward by aerodynamic drag (Hayashi 1985; Cuzzi and Zahnle 2004):
 - (a) This can increase the solid/gas ratio at some other place in the nebula closer to the Sun. Gravito-aerodynamic processes can then trigger planetesimal accumulation at the place they drifted to.
 - (b) The supervolatile-enriched snowballs can themselves be the pebbles in pebble accretion (Ormel 2017; Johansen and Lambrechts 2017) of a gas giant.

- (c) The supervolatile-enriched snowballs could evaporate when they reach warmer climates, increasing the local Ar/He (e.g.) ratio in the nebular gas (Cuzzi and Zahnle 2004; Guillot and Hueso 2006). The supervolatile-enriched nebular gas can then be captured by the gas giants when they acquire their envelopes.

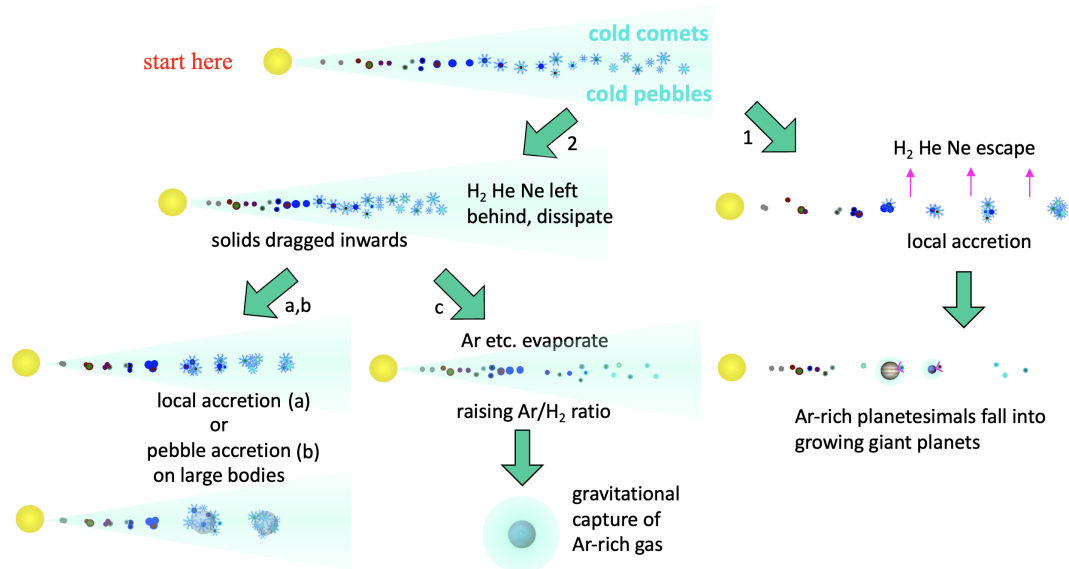


Figure 2. Some possible pathways to concentrating super-volatile elements in gas giants. These are described in the text. In the figure, argon serves as a proxy for all the super-volatile elements.

Jupiter’s roughly uniform enhancement of the six super-volatile elements, if it indeed extends to oxygen (Li et al. 2020), supports the widely-used working hypothesis that a global metallicity is useful for characterizing gas giants in general (Thorngren et al. 2016). Metallicity was originally defined by stellar astrophysicists as the sum of all elements other than H and He. The only notable change when metallicity is applied to gas giants is that Ne is removed from the index of metals. A Uranus atmospheric probe should aim to determine if the volatile elements are characterized by uniform metallicity. It may long remain an open question whether uniform metallicity extends to the refractory elements (Stevenson 2020).

Neon does not condense at solar nebular temperatures. Hence the null hypothesis is that Ne/He and $^{20}\text{Ne}/^{22}\text{Ne}$ should be solar in Uranus’s atmosphere. Neon is much

depleted in Jupiter’s atmosphere because it follows helium raindrops into the abyss (Wilson and Militzer 2010). If we accept that equations of state are imperfectly understood, we must allow for the possibility that neon could be depleted in the Uranian atmosphere. In principle neon can be separated by gravity from hydrogen and helium during hydrodynamic dissipation of the nebula, and thereby enhanced in the residual gases captured by Uranus (e.g., Mandt et al. 2020). In practice escape fluxes were likely much too big and gravity too weak to leave a measurable effect. Quantitative arguments are briefly discussed in Appendix A.

2.2. *Uranus inspired by Comet 67P/Churyumov-Gerasimenko*

The only other well-characterized source of outer solar system noble gas abundances is Comet 67P/Churyumov-Gerasimenko (Marty et al. 2017; Rubin et al. 2018, 2019). Comet 67P/C-G was born in a warmer climate than the solids that evaporated in Jupiter’s atmosphere. In particular, Ar and Kr are significantly depleted in 67P/C-G, although much less so than they are in carbonaceous chondrites. As we do not see sharp condensation temperatures preserved in moderately volatile elements in meteorites, we should not expect to find a single temperature describing partial condensation in a comet either. That said, the Ar and Kr in 67P/C-G appear to have been collected at temperatures warm enough that neither were native ices, although they may perhaps have guested in clathrates.

Unlike Ar and Kr, Xe is present in 67P/C-G at a substantial fraction of its nominal solar abundance. Rubin et al. (2018) report that the Xe/H₂O ratio in 67P/C-G’s atmosphere was $2.4 \pm 1.1 \times 10^{-7}$. For solar abundance, we follow Lodders (2020), who recommends O/Si and Xe/Si ratios of 16.6 and 5.5×10^{-6} , respectively. At solar abundances, about 20% of the oxygen is expected to be in refractory oxides. Using 67P/C-G volatile abundances tabulated by Rubin et al. (2019), 83% of volatile oxygen is in H₂O. If we allow another 5% of the oxygen to reside in more refractory organic materials, the expected solar Xe/H₂O ratio would be $5.5 \pm 2 \times 10^{-7}$. Therefore, to first approximation, 67P/C-G is depleted in Xe with respect to the Sun by only a factor of two or three. That a large fraction of the Xe originally in the gas condensed is an important constraint when weighing the meaning of xenon’s enormous isotope anomalies, as these cannot be explained as an exotic trace phase, nor in any simple way as a highly fractionated remnant. The isotopes will be discussed in detail in Section 4.

If warm comets resembling 67P/C-G were more important volatile sources for Uranus than for Jupiter, the different inheritances should be clearly visible in Ar, Kr, and Xe. Figure 1 plots the predicted Ar, Kr, and Xe abundance patterns that would

result if comets like 67P/C-G were the major source of volatiles. Two predictions are plotted. The lower estimates (green squares) presume that the true bulk 67P/C-G C/O ratio is solar. The higher estimates (black diamonds) scale volatile abundances to the subsolar C/O ratio observed in 67P/C-G’s evaporated materials (Mandt et al. 2020). The predicted Xe abundance on Uranus is comparable to what it would be if the source were cold comets. But the Kr/O and Kr/Xe ratios in 67P/C-G are distinctly subsolar, and the Ar/O ratio is very subsolar; indeed, the predicted Ar/He ratio on Uranus would only slightly exceed the solar ratio, because very little of Uranus’s Ar would have been collected in solids. Such a noble gas pattern if seen might imply that Uranus was closer to the Sun than was Jupiter when Uranus captured its envelope, or that accretion of Uranus predated envelope capture by Jupiter, or something else weirder still.

3. NOBLE CLOUDS

Uranus is cold enough, and if any of our arguments for xenon’s abundance hold, xenon is abundant enough that it should condense, a possibility that seems to have been overlooked (e.g., Moses et al. 2020). Expected methane and xenon clouds are illustrated in Figure 3.

In Figure 3 we use a p - T profile from Sromovsky et al. (2011), which for $p < 1$ bar is essentially identical to the p - T profile found by Lindal et al. (1987). For the vapor pressures of noble gases we fit a simple Antoine equation

$$\log_{10} P_{\text{sat}} = A - \frac{B}{T + C} \quad (1)$$

to sublimation vapor pressure data plotted by Ferreira and Lobo (2008). Our Antoine parameters for Xe, Ar, Kr, and CH₄ are listed in Table 1. For CH₄ we fit Antoine parameters for the vapor pressure over the solid that were originally published by Karwat (1924). There must be data somewhere that go to lower T , but our fit is adequate for our purposes.

Condensation occurs when the saturation temperature is higher than the ambient temperature. The saturation temperature of a gas for a given partial pressure P is obtained by inverting Eq 1

$$T_{\text{sat}} = \frac{B}{A - \log_{10} P} - C. \quad (2)$$

Saturation temperatures for Ar, Kr, Xe, and CH₄ are plotted against the nominal Uranian p - T profile in Figure 3. For CH₄ condensation we assume a 4% mixing ratio

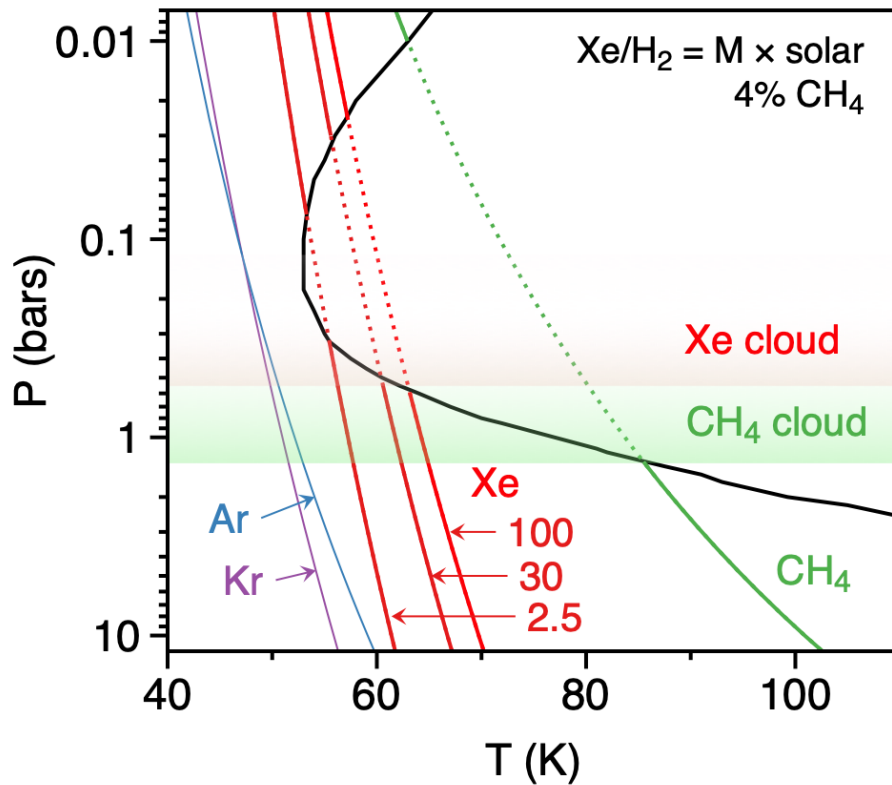


Figure 3. Xenon clouds. The plot compares condensation temperatures to a nominal p - T profile of Uranus (Sromovsky et al. 2011). Condensation occurs when the ambient temperature is colder than the condensation temperature. For methane we assume a 4% volume mixing ratio below the cloud base. For Xe we show three different abundances: 100 \times , 30 \times , and 2.5 \times solar. Xenon is expected to condense in all three cases. For Ar and Kr condensation we show only the highest abundance 100 \times solar cases.

Table 1. Antoine parameters used here

Species	A	B	C	T_{min}	T_{max}	Reference
CH ₄	4.18	439	-5	77	110	Dortmund Data Bank ^a
Ar	4.63	380	-4	37	85	(Ferreira and Lobo 2008)
Kr	5.735	671.3	4	37	90	(Ferreira and Lobo 2008)
Xe	3.74	633	-8	50	90	(Ferreira and Lobo 2008)

^a – DDB’s reference for vapor pressure over methane ice is Karwat (1924).

below the clouds. For Ar and Kr we assume a high abundance of $100\times$ solar in order to maximize their chances of condensing. For Xe we plot enhancements of 100, 30, and 2.5 times solar. These correspond to volume mixing ratios of 31, 9, and 0.8 ppbv, respectively. For any plausible abundance, Xe is expected to condense as an ice. For 10 ppbv ($33\times$ solar), Xe condenses at $T \sim 61$ K at altitudes above ~ 0.5 bars. Because it condenses, there should be no expectation that Xe is uniformly mixed below the clouds. Given xenon’s very low abundance, it seems likely that condensation is on methane ice grains or other available particles rather than as pure clouds.

3.1. *Xe fractionation in condensation*

Condensation can cause fractionation. At 60 K, the difference in vapor pressures between ^{130}Xe and ^{136}Xe is expected to be of the order of 1‰, using data and equations given by [Alamre et al. \(2020\)](#). At peak condensation, only 2% of Xe remains in the vapor phase for a nominal $40\times$ solar enhancement, which implies that the vapor’s $^{136}\text{Xe}/^{130}\text{Xe}$ ratio could be enriched $\sim (1/0.02)^{0.001} \sim 4‰$ by Rayleigh distillation. This is very small compared to the typical magnitude of Xe’s isotopic fractionations (see below) or the plausible capabilities of any Uranus Probe instrument. We conclude that isotopic fractionation during condensation of Xe is unlikely to be important.

3.2. *Ar and Kr*

As shown in [Figure 3](#), neither argon nor krypton condense in the nominal atmosphere, even if we assume high end enhancements of $100\times$ solar. This makes them the most useful elements for assessing the role of cold comets. If Uranus accreted its envelope of highly volatile elements from the same reservoir from which Jupiter accreted its envelope, the Ar/Kr ratio would be solar and the Ar/H₂ ratio would be enhanced over solar by a factor of order 30 – 100. The expected abundance pattern is shown by the red open circles in [Figure 1](#). If instead Uranus accreted its noble gases as warm comets resembling 67P/C-G, the Ar/Kr and Kr/Xe ratios would be subsolar and the Ar/H₂ ratio would be solar. This abundance pattern is shown by the open green and black symbols in [Figure 1](#).

It may be possible that the Uranian winter poles get cold enough for Ar and Kr to condense. [Figure 3](#) shows that condensation near the tropopause becomes possible if Ar and Kr abundances are at the high end of our predictions (~ 500 ppmv Ar) and ambient temperatures fall below ~ 48 K. If Ar and Kr do condense, they too might not be globally mixed. Also, if Ar does condense, it must be abundant, and therefore

its clouds should be relatively substantial. Polar argon clouds might be detectable remotely as spring approaches, or from an orbiter via stellar occultation.

4. XENON ISOTOPES

Xenon’s nine stable isotopes vary enormously in the Solar System and often display very large signals, which make them excellent targets for a Uranus atmosphere probe. Figure 4 plots selected Xe isotopic data. The upper panel plots abundances of the different isotopes normalized to ^{132}Xe , while the lower panel renormalizes the data to solar abundances, which facilitates comparing patterns. The selection includes the Sun (through the solar wind, Meshik et al. 2020); average carbonaceous chondrites (AVCC, Pepin 1991); the ubiquitous Phase Q (Busemann et al. 2000); Jupiter as measured by the Galileo Probe (Mahaffy et al. 2000); comet 67P/C-G (Marty et al. 2017); Earth’s air; and U-Xe (air’s primary Xe, Pepin 2000). These particular xenons were selected to tell a story.

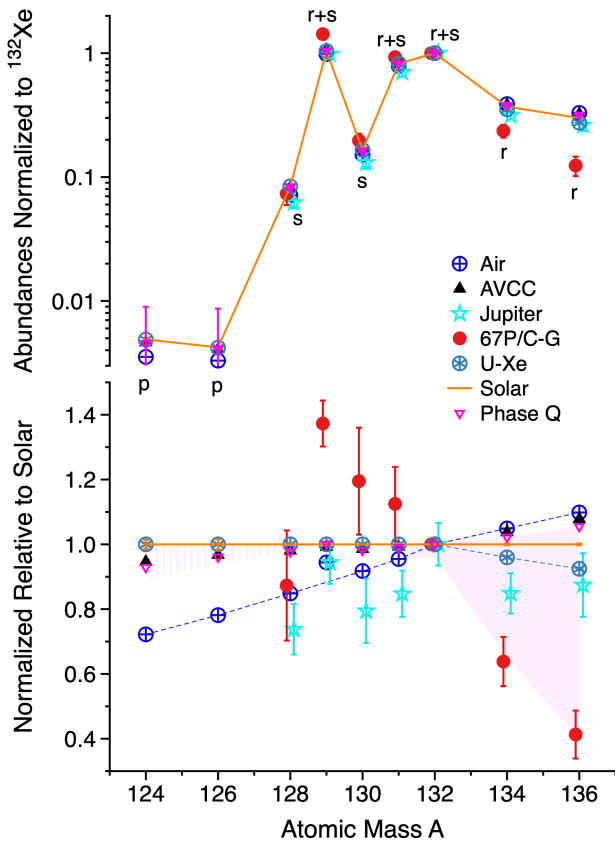


Figure 4. Selected xenon isotopes in the Solar System. In the top panel abundances are normalized to ^{132}Xe . This shows which nuclei are favored by nucleosynthesis. Nucleosynthetic sources of each isotope are indicated: “r” for rapid neutron addition and “s” for slow, and “p” for rapid proton addition. U-Xe is the reconstructed birth composition of Xe in air (Pepin 2000). Phase Q and AVCC-Xe are representative of carbonaceous chondrites (Pepin 1991; Busemann et al. 2000). The bottom panel renormalizes the top panel to solar abundances, which facilitates comparing patterns. The Xe in comet 67P/C-G stands out as being rich in the partially radiogenic ^{129}Xe (^{129}I , 15.7 Myr half-life, also r+s) and being extremely deficient in the heavy r-only isotopes ^{134}Xe and ^{136}Xe (Marty et al. 2017). Pink shading suggests the range of what might be found on Uranus.

Meteorites are diverse and the noble gases found in them even more diverse (Gilmour 2010; Marty 2022). Here we opt for a greatly oversimplified discussion. Much of the Ar, Kr, and Xe in chondrites is found in a refractory organic material called Phase Q (Busemann et al. 2000). Compared to the solar wind, all 3 heavy noble gases (Ar, Kr, Xe) are isotopically mass fractionated in Phase Q by about $\sim 1\%$ per amu, with heavier isotopes preferred and heavier elements very strongly preferred. The mass fractionation can be ascribed to many possible causes. Three of note are ion chemistry during synthesis of organic matter (Frick et al. 1979; Kuga et al. 2015, 2017); gravitational settling within porous planetesimals (Ozima and Nakazawa 1980; Zahnle et al. 1990); and fractionation during escape, probably from the planetesimal itself (Benedikt et al. 2020).

Average carbonaceous chondritic Xe (AVCC Xe) is distinctly less mass fractionated ($\sim 0.6\%$ per amu) than Phase Q, but it is also enriched in Xe’s two heaviest isotopes (Gilmour 2010; Mandt et al. 2020). The excess ^{134}Xe and ^{136}Xe is called Xe-H. When allowance is made for mass fractionation, AVCC Xe is also seen to be enriched in the light isotopes ^{124}Xe and ^{126}Xe . The excess of ^{124}Xe and ^{126}Xe is known as Xe-L. When the H and L excesses occur together, as they usually do in meteorites, the excesses are known as Xe-HL. Xe-HL is carried in presolar grains, chiefly nanodiamonds, silicon carbides, and graphite (Huss et al. 2008; Ott et al 2012; Mandt et al. 2020). Many meteorites loosely resemble AVCCs in these ways (Huss et al. 1996), although the mass fractionations in enstatite chondrites and ureilites are smaller than in AVCCs, and some enstatite meteorites (e.g., the aubrite Pesyanoe) carry solar Xe.

Atmospheric Xe is very strongly mass fractionated and polluted with radiogenic debris, but its real strangeness lies in its being deficient in the heavy isotopes ^{134}Xe and ^{136}Xe compared to the Sun. Atmospheric Xe evolved by addition of spontaneous fission of ^{244}Pu (80 Myr half-life) and by preferential escape of light isotopes over the course of 2 billion years (Avice et al. 2018; Zahnle et al. 2019). One reconstructs Earth’s original Xe—called “U-Xe”—by reversing this history (Pepin 1991, 2000). How this is done is sketched out in Appendix B. It is notable that U-Xe does not appear to have been deficient in the light isotopes ^{124}Xe and ^{126}Xe ; i.e., Earth is deficient in Xe-H but not in Xe-L. U-Xe had been very hard to understand: it seemed impossible to subtract Xe-H from Earth to turn solar Xe into U-Xe, and it is impossible to add a small sprinkling of exotic stardust to a Sun-sized reservoir of U-Xe to change it into solar Xe.

Results from the Rosetta mission to Comet 67P/C-G, when taken at face value, provide the key to unlocking U-Xe (Marty et al. 2017; Rubin et al. 2018). The xenon evaporating off comet 67P/C-G qualitatively resembles U-Xe in its deficiency of ^{134}Xe

and ^{136}Xe , but the magnitudes of the isotope anomalies in 67P/C-G are truly gigantic (Figure 4). If one neglects ^{128}Xe (which is relatively rare and suffers from confusion with S_4), the reported data could be fit to an extreme negative mass fractionation of the order of -14% per amu. Malfunction seems unlikely: the instrument also returned a wholly credible measurement of an on-board Xe calibration sample (Marty et al. 2017). Fractionation also seems unlikely: the nearly solar Xe/ H_2O ratio in 67P/C-G’s vapors implies that we are looking at a large fraction of the comet’s original xenon, rather than at a highly fractionated tail of something that had once been much more abundant. Nonetheless, one might be tempted to conjure an *ad hoc* mechanism for grossly fractionating Xe were it not for the fact that 67P/C-G’s xenon resolves the mystery of U-Xe.

If we accept the Rosetta data, Xe in 67P/C-G is either extremely deficient in ^{134}Xe and ^{136}Xe or it is extremely enriched in $^{129}\text{Xe} - ^{132}\text{Xe}$. For convenience, we will abbreviate the strange Xe of 67P/C-G as “CG-Xe” (most single letters of the alphabet are already taken). Within the generous uncertainties, it is possible to create U-Xe by mixing $\sim 22\%$ CG-Xe with chondritic Xe (Marty et al. 2017). In other words, it now appears that a tributary to U-Xe does exist as a pure component in the Solar System. U-Xe itself now appears to represent a pooled average of a wider span of primary compositions, and as such may be unique to Earth.

4.1. Nucleosynthetic xenon

The differences between 67P/C-G and the solar nebula are almost certainly nucleosynthetic. Nucleosynthesis in elements heavier than iron is categorized by process. The p-process refers to rapid proton addition, the r-process to rapid neutron addition, and the s-process to slow neutron addition (Arnould et al. 2007; Käppeler et al. 2011). Xenon is usually classified as an r-process element (Arnould et al. 2007), but because it has nine stable isotopes, the full story is more complicated: there are at least two r-processes, many s-processes, and a p-process (Gilmour and Turner 2007; Marty et al. 2017; Avice et al. 2020). Figure 4 indicates the processional source or sources of each of the isotopes.

The main r-process creates a prominent abundance peak centered on ^{128}Te , ^{129}I (which eventually decays to ^{129}Xe , $\tau_{1/2} = 15.7$ Myrs), ^{130}Te , and ^{131}Xe (Arnould et al. 2007). It is responsible for ^{129}Xe , ^{131}Xe , and much of ^{132}Xe . The neutron-rich isotopes ^{134}Xe and ^{136}Xe (Xe-H) are made at least in part by a different r-process because, as clearly seen in Figure 4, the abundances of ^{134}Xe and ^{136}Xe scale independently of the main r-process. Gilmour and Turner (2007) and Avice et al. (2020) call this other r-process the “h-process” to reflect its special role in forging Xe-H.

The s-process is usually held uniquely responsible for ^{128}Xe and ^{130}Xe because direct r-process formation is blocked by stable ^{128}Te and ^{130}Te , respectively. However, the s-process is contingent on the starting composition (Käppeler et al. 2011). For example, neutron capture by ^{129}Xe creates ^{130}Xe . Thus the relatively high abundance of ^{130}Xe in 67P/C-G seems to imply that the s-process acted on a glut of main r-process isotopes. When this observation is reconciled with the depletion of ^{134}Xe and ^{136}Xe , it seems reasonable to describe CG-Xe as being s-process enriched (Marty et al. 2017; Rubin et al. 2018).

The light isotopes ^{124}Xe and ^{126}Xe (Xe-L), which are very rare, must be made by a p-process. Correlated excesses of heavy and light Xe isotopes are prominent in presolar diamonds (Ott et al 2012). For our purposes, the H-L correlation is something to look for on Uranus. Hence we have sketched in pink a possible p-process deficit on Uranus in Figure 4. Because the p-process nuclei are rare, they may set a performance floor on the Probe.

4.2. *Strange xenon in the solar system and beyond*

The simplest classification scheme is a ternary plot with the Sun, presolar grains (PSG), and 67P/C-G as vertices (Figure 5). Chondrites appear to have captured nebular xenon resembling Phase Q in organic matter. This xenon was mass fractionated to varying degrees by processes probably linked to the capture process itself. Presolar grains added excess Xe-HL to chondrites. The third distinct reservoir seen in 67P/C-G and Earth’s air is labeled “CG67” on Figure 5. Earth’s original Xe (U-Xe) can be described as a solar base with addition of $\sim 14\%$ 67P/C-G-like xenon, or as an AVCC-like base with addition of $\sim 22\%$ 67P/C-G-like xenon (Marty et al. 2017).

A relationship, if any, between the end-member reservoirs seen in Xe and the more familiar NC/CC isotopic dichotomy seen in refractory inner solar system materials is unclear. The general trend may be the same, as s-process nuclei seem more prominent nearer the Sun, and both trends could be consistent with a late infall of s-process-rich material on the inner solar system (Nanne et al. 2019). However, the amplitude of the trend in Xe is orders of magnitude larger. The different xenons might characterize nebular reservoirs on larger spatial or temporal scales than the NC/CC dichotomy.

The nucleosynthetic anomalies seen in 67P/C-G’s xenon are so large that they almost seem to have come from another solar system. One way to account for the strange composition of 67P/C-G would be if it had been scattered out of, or captured from, another solar system in the Sun’s birth cluster. This other solar system would by construction have precipitated out of a different local mix of stellar effluents.

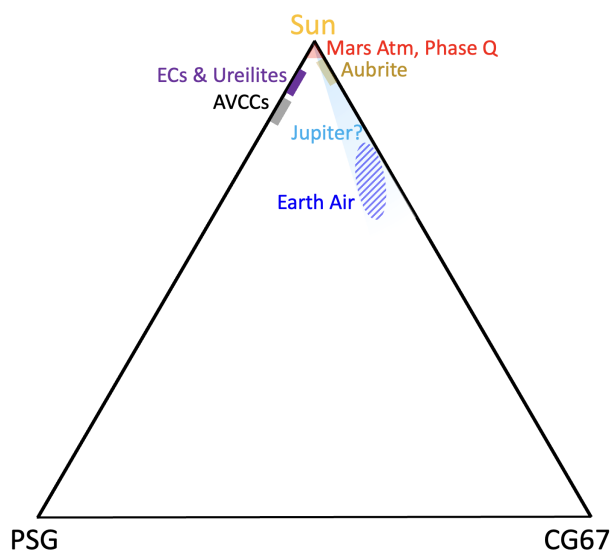


Figure 5. A schematic ternary plot of Xe in the solar system. The three vertices—solar, presolar grains (PSG), and comet P67/C-G—represent isotopic anomalies that can only be explained by distinct nucleosynthetic reservoirs. Earth’s birth Xe (U-Xe) is of mixed parentage. Data for enstatite chondrite (EC, S. Oman), aubrite (Pesyanoe), and AVCC are from [Pepin \(1991\)](#); the ureilite and Phase Q are from [Busemann et al. \(2000\)](#); Mars ([Péron and Mukhopadhyay 2022](#)). All reservoirs other than P67/C-G have been corrected for evident mass fractionation. Jupiter is extremely uncertain but intriguing.

Another possibility would be if the Sun accreted a fresh cloud of gas after the original solar nebula had dissipated, sparking a second burst of planetesimal formation within the solar system starting from a different base composition. A third option inverts the chronology: perhaps CG67 condensed extremely early, *before* the solar nebula was enriched by adding a fresh injection of Xe-H-rich gas.

The origin of the different xenons remains a mystery. AGB stars are known sites of s-process nucleosynthesis ([Käppeler et al. 2011](#)). Strange xenon in 67P/C-G could record effluent from an AGB star that had no chance to mix with the solar nebula’s other materials. There are planetary nebulae observed to be enriched in Xe by an order of magnitude, which is ascribed to s-process nucleosynthesis in the particular AGB star that is now shedding its atmosphere ([Sharpee et al. 2007](#)). It is also plausible that 67P/C-G Xe was relatively young. Youth is suggested by the anomalously high abundance of ^{129}Xe in CG-Xe, which can be explained if 67P/C-G captured live ^{129}I more efficiently than it captured Xe ([Marty et al. 2017](#); [Avice et al. 2020](#)).

As [Marty et al. \(2017\)](#) emphasize, it takes very little CG-Xe to make a big mark on Earth’s Xe, because Xe is very abundant in 67P/C-G. Hence the signature of 67P/C-G-like material in Earth is expected to be very small in more refractory elements, including water. Nonetheless, what is valid for Xe will be valid to some extent for other elements. Subtle terrestrial isotopic anomalies, such as those seen in ancient cratonic ruthenium ([Fischer-Gödde et al. 2020](#)), could stem from the same s-process-

rich source as Earth’s strange xenon. Non-solar abundances might not be limited to heavy elements. Carbon in particular is linked to s-process synthesis in AGB stars because the neutrons come from ^{13}C (Käppeler et al. 2011), which hints that the C/O ratio may not have been the same everywhere in the solar system. It is possible that Uranus’s composition was affected.

4.3. *Krypton*

Krypton’s isotopic patterns are muted compared to xenon’s (Figure 6). As noted above, Kr’s isotopes, like Xe’s, are mass fractionated by as much as 1% per amu in Phase Q and many chondrites. Krypton also shows some small isotopic anomalies, chiefly in ^{83}Kr and ^{86}Kr . These show as deficits in 67P/C-G. Earth’s mantle also shows a small deficit in the neutron-rich isotope ^{86}Kr (Péron et al. 2021), which parallels what is seen in xenon. Small ^{83}Kr *excesses* are sometimes seen in interstellar grains (Huss et al. 2008) that are enriched in Xe-H, a mirror image pattern that also parallels what is seen in xenon. Krypton is made by multiple s-processes (both main and “weak,” each with several options for branching), an r-process, and a p-process (Käppeler et al. 2011). It is therefore not surprising to see different nucleosynthetic patterns in different materials. Rubin et al. (2018) and Avice et al. (2020) devise detailed mixing models involving both Kr and Xe and multiple nucleosynthetic sources. In these models, 80% of the Xe in 67P/C-G is novel but only 5% of the Kr is. If so, it is plausible that the gas 67P/C-G accreted from had an elevated Xe/O ratio, which supports the hypothesis that ^{129}I was alive when 67P/C-G accreted.

4.4. *Jupiter, again*

There is a slight hint of ^{134}Xe and ^{136}Xe deficiency in Jupiter, seen in Figure 4. Although the data aren’t precise enough to warrant any conclusions, one could easily imagine that one is seeing a 10% contribution from 67P/C-G-like Xe, which is where we plot Jupiter on Figure 5. Obtaining a clear picture of Xe isotopes on Uranus could go a long way toward sorting out the role of 67P/C-G-like and the importance of alternative cosmic abundances in the Solar System.

5. CONCLUSIONS

Noble gas elemental abundances and Xe isotopes have much to say about the cosmic provenance of Uranus if we take the opportunity to ask. Argon and krypton elemental abundances will reveal the extent to which Jupiter’s envelope’s apparently uniform abundances of C, N, S, Ar, Kr, and Xe translate to an ice giant, and they provide a solar system test of the astrophysically convenient metallicity hypothesis

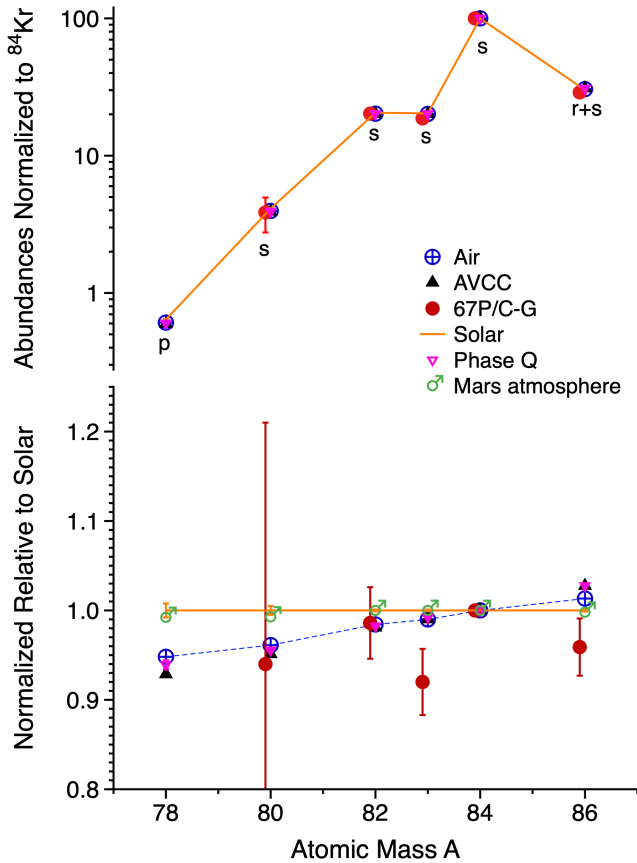


Figure 6. Krypton isotopes in the Solar System: abundances and nucleosynthetic sources. The top panel normalizes abundances to ^{84}Xe . This shows which nuclei are favored by nucleosynthesis. The bottom panel is normalized to solar abundances, which facilitates comparing patterns. Phase Q, AVCC-Xe (Pepin 1991; Busemann et al. 2000), and air are similar—all are mass-fractionated with respect to the Sun, although air slightly less so. Mars’s atmosphere is solar and its interior appears chondritic (Péron and Mukhopadhyay 2022). 67P/C-G appears to show distinct nucleosynthetic anomalies (Rubin et al. 2018).

(c.f., Thorngren et al. 2016). Neon, if it should prove overabundant, would provide a window into the mechanism by which Uranus attracted its nebular envelope.

Xenon condensation is an anticipated feature of Uranus. As seen with ammonia on Jupiter, the true abundance of a condensible gas in a gas giant is likely to be variable and hence difficult to determine with any confidence (Guillot et al. 2020). A single probe may give a misleading picture of xenon’s abundance, even for measurements taken below the clouds. Instead, xenon becomes a tracer of cloud dynamics and atmospheric circulation, which is not a role obviously well suited to a species that in practice cannot be mapped. On the other hand, condensation concentrates Xe much more effectively than a noble gas enrichment cell. The clouds present an opportunity for precisely measuring Xe’s isotopes that a suitably designed probe could exploit; in effect, by doing intentionally what the Pioneer Venus Probe did accidentally for D/H (Donahue et al. 1982).

What can be learned from Xe’s isotopes? To first approximation, xenon’s isotopes appear to track three distinct reservoirs of solar nebular gas. One resembles the Sun and, when mass fractionated, many chondrites. A second, found in presolar grains, tracks a particular style of nucleosynthesis that favors the most proton-rich and most neutron-rich isotopes, and then binds them in refractory carbon-rich grains. The second source exists only in trace amounts in the inner solar system and is not expected to be measurable on Uranus. The third source is present at nearly solar abundance in 67P/C-G, but is also discoverable in Earth’s air. Xenon’s high abundance in 67P/C-G suggests that, like the solar nebula, the third source was condensed from a gas. It is an intriguing observation that the third source is highly depleted in Xe’s heavy r-process-only isotopes (Xe-H) in approximate mirror image to how those same isotopes appear enriched in the presolar grains. The mirror image relationship does not extend to the proton-rich nuclei. There is an underlying story behind this pattern that has yet to be told.

When we focus in on 67P/C-G as a tracer of the third source, we see hints of new matter being added at a relatively late time in the solar nebula’s evolution. The very high ^{129}Xe in 67P/C-G can be explained if iodine condensed more efficiently than xenon — in itself a reasonable request — provided that the gas the comet condensed from was young enough that the newly synthesized ^{129}I (15.7 Myr half-life) had yet to decay. In other words, the gas was young when 67P/C-G was made. Whether comets like 67P/C-G condensed within our solar system in a late burst of planetesimal accretion, or whether they fell fully formed from some other solar system, are open questions.

It is to be determined if the third source contributed significantly to Jupiter and Uranus. Xenon’s isotopic anomalies in the Solar System are big enough to suggest that something interesting ought to be detectable in Uranus, and when found, will reveal how the nucleosynthetic sources of Uranus’s materials resemble or differ from those of the inner solar system, Jupiter, or even the Sun itself.

Acknowledgments. We thank two anonymous referees for their thoughtful and substantive reviews, as well as for their advice on what it should be called. This research did not receive any specific grant from funding agencies in the public, commercial, or not-for-profit sectors.

APPENDIX

A. ON NEON

It has been suggested that noble gases could have been mass fractionated during the photoevaporative hydrodynamic escape of hydrogen and helium from the nebula (Mandt et al. 2020). Because Ne is heavier than H₂ and He, it can fall behind during dissipation of the nebula, which would make Ne in the remnant of the nebula more abundant and isotopically heavier. Neon in Uranus’s atmosphere might keep a record of these events. However, diffusive separation is difficult because the gravitational force responsible for diffusive separation would be weak (Guillot and Hueso 2006). To quantify the discussion, it is helpful to construct an example of diffusive separation of Ne in an escaping hydrodynamic wind of nebular gases.

The cross-over mass m_c is defined as the heaviest isotope that can escape in a hydrodynamic wind. If $m < m_c$, the efficiency of escape is proportional to $m_c - m$. By definition, there is no escape if $m > m_c$. The cross-over mass for neon can be approximated by (Hunten et al. 1987)

$$m_c = m_n + \frac{\phi k_B T N_{\text{Avo}}}{g b_{n,\text{Ne}}}, \quad (\text{A1})$$

where $m_n \approx 2.4$ amu is the mean molecular weight of the nebular gas and $m_{\text{Ne}} = 20$; $b_{n,\text{Ne}} \approx 4.3 \times 10^{17} T^{0.74} \text{ cm}^{-1}\text{s}^{-1}$ is the binary diffusion coefficient between Ne and the nebular gas (it is nearly the same for Ne and either H₂ or He, Marrero and Mason 1972); and $N_{\text{Avo}} = 6.022 \times 10^{23}$ is Avogadro’s number. The fractionation factor, used in Rayleigh distillation, is the ratio of escape probabilities of two species of different mass,

$$x_{n,\text{Ne}} = \frac{m_{\text{Ne}} - m_n}{m_c - m_n} \geq 0. \quad (\text{A2})$$

Gravity is approximated by $g = GM_{\odot}z/R^3$, where M_{\odot} is the mass of the Sun, R is the radial distance from the Sun, and z is the height above the disk plane. To complete the illustration, take $R = 10$ AU and $z/R = 0.2$, for which $g \approx 10^{-3} \text{ cm s}^{-2}$. The escaping flux ϕ_n of H₂ and He can be estimated from the total amount of material that needs to escape divided by the area from which it escapes and the time taken to escape. We might expect escape of a Jupiter’s mass of material from an annulus of width $\Delta R = 0.2R$ over 5 million years. With these choices,

$$\phi_n = 1.1 \times 10^{11} \left(\frac{M}{M_{\text{Jup}}} \right) \left(\frac{5 \text{ Myrs}}{t} \right) \left(\frac{20 \text{ AU}^2}{R \Delta R} \right) \text{ cm}^{-2}\text{s}^{-1}. \quad (\text{A3})$$

The crossover mass would then be $m_c \approx 4.4 \times 10^4 (T/30)^{0.26}$, which is so high that very few neon atoms would be left behind. The fractionation factor between Ne and the hydrogen/helium is $x_{n,Ne} \approx 0.0004$. If Uranus captured the last 0.3% of a Jupiter’s mass of gas, we can use Rayleigh distillation to estimate that the Ne/H₂ ratio would be raised by a factor $300^{0.0004} = 1.0023$, which is quite negligible.

Nor is neon expected to fractionate on infall: accretion of an Earth mass of nebular gas over 3 million years on Uranus corresponds to an influx $\phi_n \sim -2 \times 10^{17} \text{ cm}^{-2}\text{s}^{-1}$, which for $g = 1000 \text{ cm s}^{-2}$ implies a crossover mass of order 10^5 amu. To achieve significant enhancements of Ne/H₂ or ²²Ne/²⁰Ne by diffusive separation of gases requires much more modest flows acted on by a strong gravitational field, as might be possible from a slowly dissipating, relatively low mass heliocentric torus not too distant from the Sun. As such a scenario is not wholly unimaginable, neon may hold surprises.

B. ON U XENON

Earth is markedly deficient in xenon’s r-process-only heavy isotopes ¹³⁴Xe and ¹³⁶Xe, although this fact is hidden under the mass-dependent fractionation that also characterizes atmospheric Xe. By construction, U-Xe is designed to recover the composition of Xe in air before radiogenic isotopes were added and before atmospheric xenon was acted upon by fractionating escape. U-Xe was originally conceived as the true solar Xe, then later as a kind of Xe that existed in pure form somewhere in the Solar System (Pepin 1991, 2000, 2006). It has not yet been found. What happened instead was that Rosetta revealed in 67P/C-G a world in which the depletions of ¹³⁴Xe and ¹³⁶Xe far exceed those of U-Xe. Evidently U-Xe was not a pure component, but rather a mixture of older components, at least one of which resembled 67P/C-G in being very deficient in ¹³⁴Xe and ¹³⁶Xe (Marty et al. 2017; Rubin et al. 2018). It now seems that U-Xe marked a stage in Earth’s early atmospheric evolution, rather than its beginning.

U-Xe is reconstructed from atmospheric xenon by (i) undoing the mass-dependent fractionation and (ii) by subtracting radiogenic Xe. The chief radioactive sources, ¹²⁹I ($\tau_{1/2} = 15.7$ Myr) and ²⁴⁴Pu ($\tau_{1/2} = 80$ Myr), are both short-lived. It is now known that half of xenon’s mass fractionation took place in the Archean between 3.5 Ga and 2.4 Ga (Avice et al. 2018; Ardoin et al. 2022), and it is reasonable to infer that much of the rest of the fractionating escape took place under similar conditions between 4.4 Ga and 3.5 Ga.

Isolating air’s small ¹²⁹Xe excess is straightforward, but thanks to the large ¹²⁹Xe excess in 67P/C-G, the classic interpretation of excess ¹²⁹Xe in the atmosphere as

^{129}I decay *in situ* on Earth (Ozima and Podosek 2002) is no longer on firm footing (Marty et al. 2017). Isolating air’s fissionogenic xenon is more challenging because fission spawns a broad spectrum of isotopes that have to be separated from mass fractionation. ^{244}Pu is predominantly an α -emitter. The branching ratio for spontaneous fission is 1.23×10^{-3} (Ozima and Podosek 2002). The Xe isotope most affected by fission is ^{136}Xe . It is produced in 5.6% of the spontaneous fissions (Ozima and Podosek 2002). It is convenient to scale fission products in relation to ^{136}Xe . Plutonium’s daughters are listed in Table B1.

Table B1. The Nine Isotopes of Xenon

j	Air ^a	SW ^b	AVCC ^c	U-Xe ^a	Pu-Xe ^d	Xe-H ^e
124	2.337 ± 0.007	2.97 ± 0.04	2.851 ± 0.051	2.928 ± 0.01	0	0
126	2.18 ± 0.011	2.56 ± 0.04	2.512 ± 0.04	2.534 ± 0.013	0	0
128	47.15 ± 0.047	51.0 ± 0.1	50.73 ± 0.38	50.83 ± 0.06	0	0
129	649.6 ± 0.58	631.4 ± 1.3	653 ± 17	628.6 ± 0.6	0.048 ± 0.055	0.196 ± 0.02
130	100	100 ± 0.34	100	100	0	0
131	521.3 ± 0.59	501.0 ± 1.2	504.3 ± 2.8	499.6 ± 0.6	0.248 ± 0.015	0.171 ± 0.015
132	660.7 ± 0.53	606.3 ± 1	615 ± 2.7	604.7 ± 0.6	0.893 ± 0.013	0.154 ± 0.01
134	256.3 ± 0.37	224.2 ± 0.6	235.9 ± 1.3	212.6 ± 0.4	0.930 ± 0.005	0.694 ± 0.01
136	217.6 ± 0.22	181.8 ± 0.5	198.8 ± 1.2	165.7 ± 0.3	1	1

a - Pepin (2006).

b - Meshik et al. (2020).

c - Pepin (1991).

d - Ozima and Podosek (2002).

e - Ott et al (2012).

Given ^{244}Pu ’s 80 Myr half-life and the expectation that early outgassing was efficient, we will assume that the fractionating escape took place after degassing of fissionogenic Xe (this is not an important restriction). We can write this formally in terms of 9-isotope vectors:

$$\mathbf{Air} = \mathcal{F}(\mathbf{U} + x\mathbf{Pu} + y\mathbf{I}). \quad (\text{B1})$$

The composition of U-Xe is recovered by de-fractionating the air and then subtracting off the radiogenic Xe

$$\mathbf{UXe} = \mathcal{F}^{-1}(\mathbf{Air}) - x\mathbf{Pu} - y\mathbf{I}. \quad (\text{B2})$$

For completeness we include ^{129}I in Eqs B1 and B2, but as ^{129}Xe maps uniquely to y , ^{129}Xe can be treated separately.

We have written fractionation as a general function \mathcal{F} . Hydrodynamic escape can generate complicated fractionation patterns (Hunten et al. 1987; Pepin 1991; Dauphas and Morbidelli 2014), but a simple expression is best here for illustration. In the limit that the crossover mass m_c (see Appendix A) exceeds the masses of all the escaping isotopes ($m_c > m_j, m_i$), fractionation in hydrodynamic escape reduces to a simple multiplier independent of m_c . For specificity we express fractionations with respect to ^{130}Xe .

$$\text{Air}_j = \exp(\eta(m_j - m_{130}))(\text{UXe}_j + x\text{Pu}_j). \quad (\text{B3})$$

The factor η in Eq B3 represents the magnitude of the fractionation. Equation B3 is trivially inverted to solve for a U-Xe:

$$\text{UXe}_j = \text{Air}_j \exp(\eta(m_{130} - m_j)) - x\text{Pu}_j \quad (\text{B4})$$

This version of U-Xe is underdetermined, because the contribution x of plutonium fission has not been specified. We can set plausible bounds on the amount of Pu-Xe. The initial solar system abundance of $^{244}\text{Pu}/^{238}\text{U} = 0.0068$ (Hudson et al. 1989), when scaled to a bulk silicate Earth uranium abundance of 21 ppb implies that the initial bulk silicate Earth abundance of ^{244}Pu was 3.0×10^{-10} [g/g]. The fractional yield for $^{244}\text{Pu} \rightarrow ^{136}\text{Xe}$ is $1.23 \times 10^{-3} \times 0.056 = 6.8 \times 10^{-5}$. Hence the total production of plutoniogenic ^{136}Xe on Earth has been 3.4×10^{11} moles. This can be compared to the 1.4×10^{12} moles of ^{136}Xe currently in the atmosphere.

Xenon’s mass fractionation was accompanied by the loss of 65%-90% of the Xe that remained after impact erosion (Zahnle et al. 2019). This would have included Pu-Xe, as very little Pu-Xe remains in the mantle (Kunz et al. 1998). With allowance for some early losses from impact erosion—impact erosion probably decimated early Earth’s noble gases (Genda and Abe 2005), but most of those losses predated ^{244}Pu decay—we expect Earth to have retained something like $\sim 15_{-7.5}^{+15}\%$ of its plutoniogenic Xe. This corresponds to $x \approx 8_{-4}^{+8}$, where x is measured in units in which the abundance of ^{130}Xe is 100. The resulting range of plausible “U-Xe” compositions is indicated in Figure B1 by pink shading. Note that this simple argument makes no reference to chondritic Xe.

Pepin (1991) originally proposed that U-Xe was the true solar Xe, which implied that putative solar Xe (e.g., “SUCOR,” Ozima and Podosek 2002) was U-Xe polluted with exotic Xe. Schematically,

$$\text{SW} = \text{UXe} + z\text{HXe}, \quad (\text{B5})$$

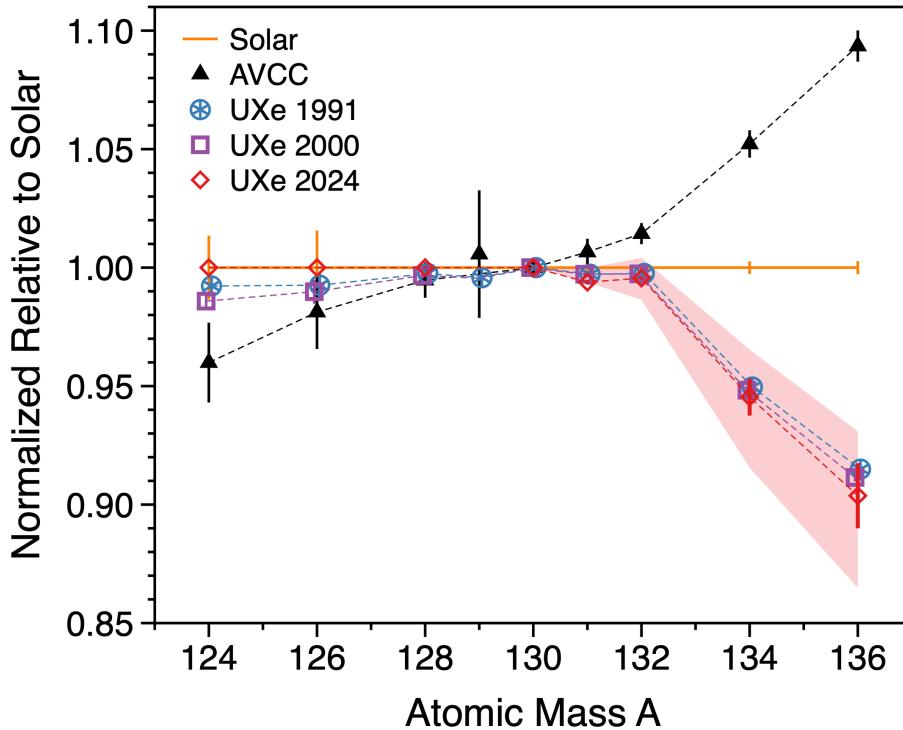


Figure B1. Reconstructed isotopic compositions of U-Xe—Earth’s birth Xe—compared to other selected xenons. The red shaded region is the range of possible U-Xe compositions consistent with plausible amounts of ^{244}Pu fission Xe in air. This derivation does *not* take chondritic Xe into account. Standard U-Xe, quoted from Pepin (1991) and Pepin (2000), uses the composition of chondritic Xe to provide additional constraints. By construction U-Xe and SW-Xe are identical for light isotopes. The differences seen here stem from revisions of the solar wind.

in which z is an optimizable parameter, and the pollutant—H-Xe—closely resembles Xe-H with ^{131}Xe mostly removed. This U-Xe is plotted on Figure B1 as “U-Xe 1991.” Later, with SW-Xe firmly established, Pepin (2000) revised the derivation of U-Xe, which in heuristic form can be written

$$\text{UXe} = \text{SW} - z\text{HXe}. \quad (\text{B6})$$

In the new derivation, H-Xe was redefined to include only ^{134}Xe and ^{136}Xe . The revised U-Xe is plotted on Figure B1 as “U-Xe 2000.”

In their details, Pepin’s derivations are rather obscure. We therefore independently performed a simple Monte Carlo simulation by taking random values from Gaussian

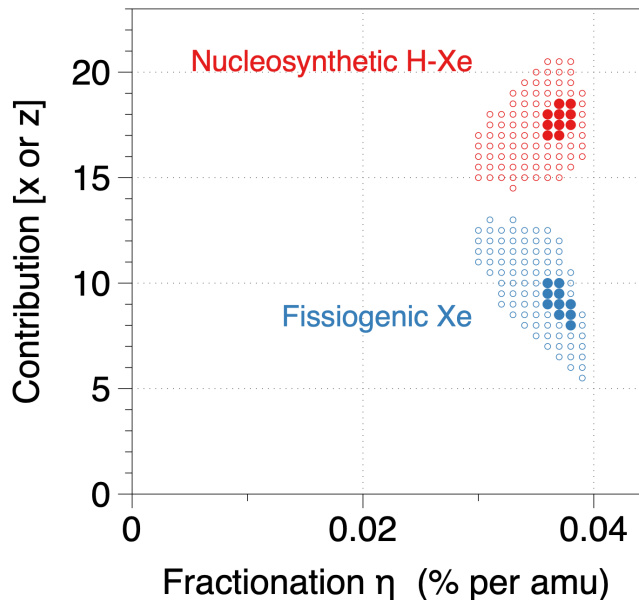


Figure B2. Reconstructing U'-Xe. Beginning with solar xenon, a quantity x of ^{244}Pu fissiogenic Xe is added and a quantity z of Xe-H is subtracted (x and z are in units where $^{130}\text{Xe} = 100$). The sum is then mass fractionated by η to generate air's Xe (η is in units of % per amu). Values of x , z , and η that give acceptable fits are plotted. The umbrae of filled disks have $\chi^2 < 1$. The penumbrae of open circles have $\chi^2 < 3.5$. The best fits are used to create a U'-Xe using Eq B6, which is plotted on Figure B1.

distributions defined by the quoted uncertainties (one σ errors are listed in Table B1). For H-Xe we followed (Ott et al 2012). Misfits were defined as

$$\Delta_j = \text{Air}_j \exp(\eta(m_{130} - m_j)) - \text{SW}_j - x\text{Pu}_j + z\text{HXe}_j. \quad (\text{B7})$$

From these we computed χ^2 values for each realization

$$\chi^2 = \sum_{j \neq 129} \frac{\Delta_j^2}{\sigma_{\text{Air}_j}^2 + \sigma_{\text{SW}_j}^2 + x^2 \sigma_{\text{Pu}_j}^2 + z^2 \sigma_{\text{HXe}_j}^2}. \quad (\text{B8})$$

Results are shown in Figure B2. For this particular numerical experiment, we find that $x = 9 \pm 3$, $z = 17.5 \pm 2.5$, and $\eta = 0.037 \pm 0.002$. This U-Xe is plotted on Figure B1 as ‘‘U-Xe 2024.’’ It is very similar to the official U-Xe, differing mostly in providing more room for uncertainties.

REFERENCES

- | | |
|---|--|
| <p>Alamre, A., Badhrees, I., Death, B.J.,
Licciard, C., Sinclair, D., 2020. ACS
Omega 5, 28977.</p> | <p>Ardoin, L., Broadley, M.W., Almayrac, et
al., 2022. Geophys. Persp. Lett. 20, 43.
Arnould, M., Goriely, S., Takahashi, K.,
2007. Phys. Rept. 450, 97.</p> |
|---|--|

- Atreya, S.K., Mahaffy, P.R., Niemann, H.B., Wong, M.H., Owen, T.C., 2003. *Planet. Space Sc.* 51, 105.
- Avice, G., Marty, B., Hofmann, A., et al., 2018. *GCA*, 232, 82.
- Avice, G., Morreira, M., Gilmour, J., 2020. *ApJ*, 889, 68.
- Benedikt, M.R., Scherf, M., Lammer, H., Marcq, E., Odert, P., Leitzinger, M., Erkaev, N.V., 2020. *Icarus* 347, article id. 113772.
- Busemann, H., Baur, H., Wieler, R., 2000. *Meteoritics Planet. Sci.* 35, 949.
- Cavalié, T., Venot, O., Selsis, F., et al., 2017. *Icarus* 291, 1.
- Cuzzi, J.N., Zahnle, K.J., 2004. *ApJ*, 614, 490.
- Dauphas, N., 2003. *Icarus* 165, 326.
- Dauphas, N., Morbidelli, A., 2014. *Treatise Geochem. Second Ed.* 6, 1.
- Donahue, T.M., Hoffman, J.H., Hodges, R.R., Watson, A.J., 1982. *Science* 216, 630.
- Estrada, P.R., Cuzzi, J.N., Morgan D.A., 2016. *Astrophys. J.* 818, 200.
- Ferreira, A., Lobo, L.Q., 2008. *J. Chem. Therm.* 40, 1621.
- Fischer-Gödde, M., Elfers, B.-M., Münker, C., et al., 2020. *Nature* 579, 240.
- Frick, U., Mack, R., Chang, S., 1979. *Proc. LPSC*, X, 405.
- Genda, H., Abe, Y., 2005. *Nature* 433, 842.
- Gilmour, J.D., Turner, G., 2007. *ApJ*, 657, 600.
- Gilmour, J.D., 2010. *GCA*, 74, 380.
- Guillot, T., Hueso, R., 2006. *MNRAS*, 367, L47.
- Guillot, T., 2019. *Unknown*. (14 pp).
- Guillot, T., Stevenson, D.J., Atreya, S.K., Bolton, S.J., Becker, H.N., 2020. *JGR*, 125, e2020JE006403.
- Hayashi, C., Nakazawa, K., Nakagawa, Y., 1985. in: Black, D.C., Matthews, M.S. (Eds.) *Protostars and Planets II*, University of Arizona Press, 1100.
- Hollenbach, D.J., Yorke, H.W., Johnstone, D., 2000. in: Mannings, V., Boss, A.P., Russell, S.S. (Eds.), *Protostars and Planets IV*, University of Arizona Press, 401.
- Hudson, G.B., Kennedy, B.M., Podosek, F.A., Hohenberg, C.M., 1989. *Proc. LPSC*, 19, 547.
- Hunten, D.M., Pepin, R.O., Walker, J.C.G., 1987. *Icarus* 69, 532.
- Huss, G.R., Lewis, R.S., Hemkin, S., 1996. *GCA*, 60, 3311.
- Huss, G.R., Ott, U., Koscheev, A.P., 2008. *Meteor. Plan. Sci.* 43, 1811.
- Johansen, A., Lambrechts, M., 2017. *Ann. Rev. Earth Planet. Sci.* 45, 359.
- Käppeler, F., Gallino, S., Bisterzo, R., Aoki, W., 2011. *Rev. Mod. Phys.* 83, 157).
- Karwat, E., 1924. *Z. Phys. Chem. (Leipzig)* 112, 486.
- Kunz, J., Staudacher, T., Allègre, C.J., 1998. *Science* 280, 877.
- Kuga, M., Marty, B., Marrocchi, Y., Tissandier, L., 2015. *PNAS*, 112, 7129.
- Kuga, M., Cernogora, G., Marrocchi, Y., Tissandier, L., Marty, B., 2017. *GCA*, 217, 219.
- Li, C., Ingersoll, A.P., Bolton, S., et al., 2020. *Nature Astron.* 4, 609.
- Lindal, G.F., Lyons, J.R., Sweetnam, D.N., Eshleman, V.R., Hinson, D.P., 1987. *JGR*, 92, 14987.
- Lodders, K., 2020. eprint arXiv:1912.00844

- Mahaffy, P.R., Niemann, H.B., Alpert, A., et al., 2000. *JGR*, 105, 15,061.
- Mandt, K.E., O. Mousis, O., Lunine, J., et al., 2020. *Space Sci. Rev.* 216, 99.
- Marrero, T.R., Mason E.A., 1972. *J. Phys. Chem. Ref. Data* 1, 2.
- Marty, B., 2022. *Icarus* 381, 115020 (12pp.)
- Marty B., Altwigg, K., Balsinger, H., et al., 2017. *Science* 356, 1069.
- Meshik, A., Pravdivtseva, O., Burnett, D., 2020. *GCA*, 276, 289.
- Moeckel, C., de Pater, I., DeBour, D., 2023. *PSJ* 4, id.25.
- Moses, J.I., Cavalié, T., Fletcher, L.N., Roman, M.T., 2020. *Phil. Trans. R. Soc. A* 378, 20190477.
- Nanne, J.A.M., Nimmo, F., Cuzzi, J.C., Kleine, T., 2019. *EPSL*, 511, 44.
- Ormel, C., 2017. in: Pessah, M., Gressel, O. (Eds.), *Formation, Evolution, and Dynamics of Young Solar Systems*, Springer International Publishing, pp. 197–228.
- Ott, U., Besmehn, A., Farouqi, K., et al., 2012. *Pub. Astron. Soc. Australia* 29, 90.
- Owen, T.C., Mahaffy, P.R., Niemann, H.B., et al., 1999. *Nature* 402, 269-.
- Ozima, M., Nakazawa, K., 1980. *Nature* 284, 313.
- Ozima, M., Podosek, F.A., 2002. *Noble Gas Geochemistry. Second Edition*. Cambridge University Press, 286 pp.
- Péron, S., Mukhopadhyay, S., Kurz, M.D., Graham, D.W., 2021. *Nature* 600, 462.
- Péron, S., Mukhopadhyay, S., 2022. *Science* 377, 320.
- Pepin, R.O., 1991. *Icarus* 92, 2.
- Pepin, R.O., 2000. *Space Sci. Rev.* 92, 371.
- Pepin, R.O., 2006. *EPSL*, 252, 1.
- Pollack, J.B., Hubickyj, O., Bodenheimer, P., et al., 1996. *Icarus* 124, 62.
- Rubin, M., Altwigg, K., Balsinger, H., et al., 2018. *Science Adv.* 4, Eaar627.
- Rubin, M., Altwigg, K., Balsinger, H., et al., 2019. *MNRAS* 489, 594.
- Sharpee, B., Zhang, Y., Williams, R., et al., 2007. *ApJ*, 659, 1265.
- Sromovsky, L.A., Fry, P.M., Kim, J.H., 2011. *Icarus* 215, 292.
- Stevenson, D.J., 2020. *Ann. Rev. Earth Planet. Sci.* 48, 465.
- Thorngren, D.P., Fortney, J.J., Murray-Clay, R.A., Lopez, E.D., 2016. *ApJ*, 831, 64.
- Venot, O., Cavalié, T., Bounaceur, R., et al., 2020. *AA* 634, A78.
- Wilson, H.F., Militzer, B., 2010. *Phys. Rev. Lett.* 104, 121101.
- Wong, M.H., Mahaffy, P.R., Atreya, S.K., Niemann, H.B., Owen, T.C., 2004. *Icarus* 171, 153.
- Youdin, A.N., Goodman, J., 2005. *ApJ* 620, 459.
- von Zahn, U., Hunten, D.M., 1996. *Science* 272, 8492.
- Zahnle, K.J., Pollack, J.B., Kasting, J.F., 1990. *GCA* 54, 2577.
- Zahnle, K.J., Catling, D.C., Gacesa, M., 2019. *GCA* 244, 56.